J Mater Sci (2011) 46:7799–7805
DOI 10.1007/s10853-011-5760-9

A practical model for the determination of transport parameters in semiconductors

J. B. Rojas-Trigos · A. Calderón · E. Marín

Received: 9 May 2011 / Accepted: 29 June 2011 / Published online: 9 July 2011

Abstract In this paper a new and practical model for the determination of transport parameters of crystalline semiconductors, by means of the photoacoustic technique is reported. The model is based on the calculation of the photoacoustic signal for the so-called heat transmission configuration, and considers that the thermal response to periodical heating, due to light absorption, in semiconductor materials has mainly two contributions: (a) the vibrations of the crystal lattice (phonon contribution) and (b) the diffusion and recombination (bulk and superficial) of the photogenerated charge carriers. Considering these contributions as the heat sources, and using unmixed Dirichlet and Neumann boundary conditions, the solution of the heat diffusion equation, necessary for the calculation of the photoacoustic signal is obtained. In addition, an expression—describing a particular transport regime—that can be used as practical fitting function, for the more available experimental conditions, is developed. Finally, values of transport parameters for silicon wafers are obtained by fitting this model to the experimental data, showing a good agreement with the values quoted in literature.

Introduction

Since the presentation of the PA technique for studying condensed matter samples by Rosencwaig and Gersho [1], numerous works have been written with the aim of providing a more complete theory that explains the experimental results in this and other related techniques. In the case of semiconductor samples, several authors have proposed different models that include the effect of the diffusion and recombination of the photogenerated charge carriers. These extra contributions lead to the inclusion of "slow" heat sources, in the sense that they appear after the "fast" heating generated by the periodical light excitation. In this direction, the earliest papers [2] have considered the bulk and surface recombination of carriers as the origin of the slow heat source, but maintaining front (illuminated surface) and rear surface recombination velocities equal. In subsequent works, this later mechanism was included, but only on the illuminated surface, for the mirage detection approach by Fournier et al. [3] and for the study of nonlinear piezoelectric PA effect by Cheng et al. [4] For the PA technique the superficial recombination in both (rear and front) surfaces has been already taken into account considering the Beer light absorption model [5–7] and the inclusion of other effects such as the thermoelastic and electronic strain contributions, among others [8, 9]. For a review of these and other major works in the field, the reader can be referred to the recent published work by Marín et al. [10].

The main difficulty in the use of the reported models, is that their implementation requires a multi parametric nonlinear fitting procedure to the experimental data (PA signal vs. modulation frequency), leading to a lack of reliability in the calculations. Thus, in this work, a photoacoustic model is proposed in which the carrier superficial recombination effect is introduced into the heat diffusion equation directly as a superficial heat source. By means of an approximation, valid for the more available experimental conditions, a special case is defined in which the general solution

J. B. Rojas-Trigos (✉) · A. Calderón · E. Marín
Centro de Investigación en Ciencia Aplicada y Tecnología Avanzada, del Instituto Politécnico Nacional, Av. Legaria # 694, Col. Irrigación, DF C.P. 11500, México
e-mail: rjosebruno@yahoo.com.mx

reduces to a more practical expression with only two adjustable parameters.

This paper is organized as follows: In "Theoretical model" section a PA signal generation model—obtained from the solution of the heat transport equation under homogenous boundary conditions—is presented. Expressions are given for particular transport regimes that can be used as a set of fitting functions for the more available experimental conditions. In "Experimental results" section, the PA signal of a set of six crystalline silicon samples are measured, and the calculated transport parameters values, by means of a non-linear least squares fitting procedure, are obtained for each sample. Our conclusions are drawn in final section.

Theoretical model

Consider an arrangement of three medium, labelled by $j = \mathrm{s}, \mathrm{b}, \mathrm{g}$, where s, b and g denote the semiconductor sample, the backing medium and the surrounding air adjacent to the illuminated face of the sample, respectively. This schema corresponds to the so-called heat transmission configuration in the PA technique (Fig. 1) in which the signal is detected at the back, i.e. the non-illuminated surface of the sample. This measurement variant offers some advantages respecting the common front detection configuration for measurement of transport properties of semiconductors, as has been discussed elsewhere [10].

When an intensity modulated light beam impinges on the surface of the semiconductor medium ($j = \mathrm{s}$), the energy of the photon is absorbed and transformed, by means of non-radiative processes, into heat (thermal energy) which propagates through the sample, heating the backing medium. Usually, in the heat transmission configuration, the backing medium is the air enclosed in the acoustic chamber of the photoacoustic cell, in which only a thin boundary layer of air adjacent to the surface of the sample responds thermally to the periodic heat flow coming from the sample, behaving like a vibratory piston and generating modulated pressure variations in the cell (with the same modulated frequency as the incident beam), i.e. the thermal energy is transformed into mechanical energy. We referred to these pressure variations as the acoustic pressure ΔP_b. The main goal in the frequency-resolved PA technique is the study of the thermal response (proportional ΔP_b), as a function of the modulation frequency. In a first approximation, the absorbed energy density can be written as follows:

$$I(\omega', x) = \frac{\sqrt{2\pi}(1-R)I_0}{2}\exp(\beta x)\,\delta(\omega' - \omega) \tag{1}$$

In Eq. 1 R is the reflection coefficient of the frontal sample's surface, I_0 is the intensity of the incident beam, $\omega = 2\pi f$ is the angular modulation frequency, x is the spatial variable in the energy flow direction and β is the optical absorption coefficient at the energy, $E = hv$ (we assumed that E is greater than the band gap energy E_g of the semiconductor). Assuming that the frequency dependency of the pressure variations ΔP_b is the same as in Eq. 1, this acoustic pressure can be detected by any adequate transduction system. This is the so-called photoacoustic signal, PAS, which is a function of the modulation frequency, and is given by the next expression:

$$\mathrm{PAS} = C_\mathrm{trans}\Delta P_\mathrm{b} \tag{2}$$

In Eq. 2, C_trans is a function dependent on the modulation frequency, characteristic of the transduction system. The absorption of the energy density I by the semiconductor ($j = \mathrm{s}$), induces an excess of (photogenerated) charge carriers, which diffuses and recombine along the sample. The photogenerated carriers give off an amount of energy ΔE to the crystal lattice equal to $E - E_\mathrm{g}$. This energy generates lattice vibrations, responsible for the appearance of a "fast" heat source, G_T in the sample. This contribution is also called the carriers thermalization mechanism. In addition to the fast heat source, the carrier recombination processes induces "slow" heat sources too. The recombination of the photogenerated carriers at the front and rear surfaces produces the superficial heat source G_SR, and the carriers recombination along the volume of the sample generate the bulk heat source G_BR. These source terms contains the influence of the electronic transport properties of the semiconductor.

Assuming the model of a bipolar semiconductor with volume and superficial carrier recombination, and a total (non-radiative) recombination lifetime, τ, independent of the carrier's excess density $n(\omega', x)$, the photogenerated carrier's density satisfy the continuity equation:

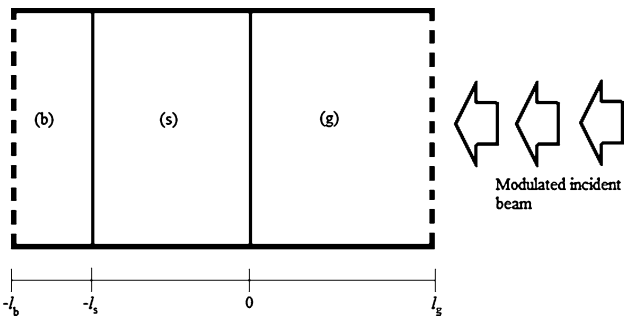

Fig. 1 Schematic photoacoustic cell geometry for the transmission configuration

$$\frac{\partial^2 n(\omega',x)}{\partial x^2} - \sigma_D^2 n(\omega',x) = -\frac{\sqrt{2\pi}(1-R)I_0\beta}{2E\,D} \times \exp(\beta x)\,\delta(\omega'-\omega) \tag{3}$$

The solution of (3) is constrained by homogenous Robin boundary conditions (also known as impedance boundary conditions) at $x = -l_s$ and $x = 0$ interfaces. Here D is the ambipolar diffusion coefficient and $\sigma_D = \mu_D^{-1}(1 + i\omega\tau)^{1/2}$, where $\mu_D = (D\tau)^{1/2}$ is the carrier diffusion length. If neither thermo-mechanical nor electromechanical coupling is present, the heat diffusion equations for the transmission configuration can be written as:

$$\frac{d^2}{dx^2}\Theta_j(\omega',x) - \sigma_j^2\Theta_j(\omega',x) = \begin{cases} -G_s(\omega',x); & j = s \\ 0; & j \neq s \end{cases} \tag{4}$$

where Θ_j are the temperature variation distributions (in the frequency domain), and $\sigma_j = (1 + i)\ \mu_j^{-1}$ is the complex thermal diffusion coefficient, which is closely related to the thermal diffusion length given by $\mu_j = (2\alpha_j/\omega)^{1/2}$. The total heat source G_s is given by:

$$\begin{aligned} G_s = G_T + G_{SR} + G_{BR} = \cdots\cdots = \frac{(1-R)\beta\Delta E}{k_s E} I(\omega',x) \\ + \frac{E_g}{k_s}[s_f n(\omega',0)\delta(x) + s_f n(\omega',-l_s)\delta(x+l_s)] \\ + \frac{E_g}{k_s}\left[\frac{n(\omega',x)}{\tau}\right] \end{aligned} \tag{5}$$

In these equations κ_s is the thermal conductivity of the sample (s), α_j is the thermal diffusivity (j = s, b, g), and s_f, s_r are the front and rear surface recombination velocities, respectively. As Eq. 5 states, the main difference between our model and other models commonly used, is the inclusion of the surface recombination contribution directly into the heat diffusion equation, and not in the boundary conditions. The solutions of equation system (4) are constrained by imposing continuity of the temperature variation distributions and the corresponding heat fluxes, at the $x = -l_s$ and $x = 0$ interfaces (Dirichlet and Neumann boundary conditions). It is also considered that the thermal effusivity of the gas is much smaller than the thermal effusivity of the sample. Consequently, it is possible to find the solutions of Eq. 4, and since the interest of this paper relies only in the heat transmission configuration, only the temperature distribution Θ_b is presented here. It lauds:

$$\Theta_b(\omega',x) = [R_s(-l_s)\exp(\sigma_b(x+l_s))]\,\delta(\omega'-\omega) \quad x \leq -l_s \tag{6}$$

$$R_s(\omega',-l_s) = -\int_{l_s}^{0} g_s(\omega',x')\frac{\cosh\sigma_s x \cosh\sigma_s(x'+l_s)}{\sigma_s \sinh\sigma_s l_s}dx' \tag{7}$$

According to the well-known thermal piston model of Rosencwaig and Gersho [1] and from Eq. 6, the expression for the acoustic pressure in frequency domain is written as follows:

$$\Delta P_b \cong \frac{\sqrt{2\pi}\,\varepsilon P_{atm} R_s(\omega',-l_s)}{l_b T_{amb}\sigma_b} = \Delta P_b^T + \Delta P_b^{SR} + \Delta P_b^{BR} \tag{8}$$

where P_{atm} is the atmospheric pressure, T_{amb} is the ambient temperature and ε is the adiabatic compressibility coefficient of the air in the acoustic chamber. The individual contributions to the acoustic pressure are denoted by ΔP_b^T, ΔP_b^{SR}, and ΔP_b^{BR} representing thermalization, surface recombination and bulk recombination, respectively, which are expressed as follows:

$$\Delta P_b^T = \frac{P_0 r_s}{1-r_s^2}\left(\frac{-r_s + (\sinh\sigma_s l_s + r_s\cosh\sigma_s l_s)e^{-\beta l_s}}{z\sinh\sigma_s l_s}\right) \tag{9a}$$

$$\begin{aligned} \Delta P_b^{SR} = \frac{E_g P_0}{D\Delta E}\Bigg\{ \frac{\delta_D}{\sigma_D(1-\delta_D^2)z\sinh\sigma_s l_s}\big[A_+\big(s_f + s_r e^{-\sigma_D l_s}\cosh\sigma_s l_s\big) + \cdots \\ A_-\big(s_f + s_r e^{\sigma_D l_s}\cosh\sigma_s l_s\big) + \big(s_f + s_r e^{-\beta l_s}\cosh\sigma_s l_s\big)\big]\Bigg\} \end{aligned} \tag{9b}$$

$$\begin{aligned} \Delta P_b^{BR} = \frac{E_g P_0 e^{-i\pi/4}}{\sqrt{2}\Delta E}\Bigg\{ \frac{a^2\,\delta_D}{(1-\delta_D^2)\sigma_D l_s z^{3/2}\sinh\sigma_s l_s}\Bigg[A_+\left(\frac{-\gamma_{sD} + e^{-\sigma_D l_s}(\sinh\sigma_s l_s + \gamma_{sD}\cosh\sigma_s l_s)}{1-\gamma_{sD}^2}\right) + \cdots \\ A_-\left(\frac{\gamma_{sD} + e^{\sigma_D l_s}(\sinh\sigma_s l_s - \gamma_{sD}\cosh\sigma_s l_s)}{1-\gamma_{sD}^2}\right) + \frac{(\sinh\sigma_s l_s + r_s\cosh\sigma_s l_s)e^{-\beta l_s} - r_s}{1-r_s^2}\Bigg]\Bigg\} \end{aligned} \tag{9c}$$

where:

$$A_{\pm} = \mp \frac{(1 \pm e_r)\left(1 + \beta D s_f^{-1}\right)e^{\pm \sigma_D l_s} - (1 \mp e_f)\left(1 - \beta D s_r^{-1}\right)e^{-\beta l_s}}{(1 + e_r)(1 + e_f)e^{\sigma_D l_s} - (1 - e_r)(1 - e_f)e^{-\sigma_D l_s}} \quad (10)$$

$$P_0 = \frac{(1 - R)\sqrt{\pi \alpha_b / \alpha_s} I_0 l_s^2 \varepsilon P_{atm}}{2^{3/2} \kappa_s l_b T_{amb}} \frac{\Delta E e^{-i\pi/2}}{h\nu} \quad (11)$$

In terms of the characteristic frequency, f_c, of the sample [11], defined as $f_c = \alpha_s (\pi l_s^2)^{-1}$, σ_D and σ_s can be rewritten, as functions of the dimensionless variable $z = f f_c^{-1}$ as follows:

$$\sigma_D l_s = a\left[1 + i\left(\frac{b}{a^2}\right)z\right]^{1/2} \quad (12)$$

$$\sigma_s l_s = (1 + i)\, z^{1/2} \quad (13)$$

where $a = l_s \mu_D^{-1}$, and $b = 2\alpha_s D^{-1}$.

In Eqs. 9a–9c, the next auxiliary coefficients were defined:

$$\begin{array}{ll} \delta_D \equiv \beta \sigma_D^{-1} & e_{r,f} \equiv D \sigma_D s_{r,f}^{-1} \\ r_s \equiv \beta \sigma_s^{-1} & \gamma_{sD} \equiv \sigma_D \sigma_s^{-1} \end{array} \quad (14)$$

The use of z instead of f as the independent variable is more convenient for a theoretical analysis, because it allows exploring the influence of the electronic transport parameters (through coefficients a and b) on the behaviour of our model for any thermal regime. In Fig. 2 the theoretical predictions for a crystalline silicon (Si) sample characterized by $E_g = 1.12$ eV, $\beta = 3 \times 10^4$ cm^{-1}, $b = 0.112$ and values of $a = 1$, 7 and 10 are shown.

Equations 9a–9c can be used to define a fitting function. However, this function will be a multi parametric one, which induces a lack of reliability on the calculations of the adjustable parameters involved.

Special case

By means of a few considerations a more practical fitting function for the PA signal can be obtained that matches with a particular experimental conditions useful in the PA technique, and that is easily achieved by almost any of PA measurement system. These are:

1. The semiconductor sample is optically opaque, this is, the sample's thickness is larger than the optical penetration skin depth, defined as $\mu_\beta = \beta^{-1}$; and therefore, $\exp(-\beta\, l_s) \approx 0$.
2. The sample is lamellar, this is, with a thickness greater to 50 μm so that for most crystalline semiconductors with low concentration of impurities, the coefficient $a = l_s \mu_D^{-1}$ satisfies the condition $a > 1$, meaning that the sample thickness is greater than the carriers diffusion length, and therefore, a negligible number of carriers recombine at the rear surface.
3. The values of the modulation frequency are above the characteristic frequency f_c, but they are not much higher than 1 kHz. In this case the signal/noise ratio still is bigger enough to ensure reliability in the measurements, and it is consistent with the requirement $1 < z \ll a^2 b^{-1}$ (equivalent to $f_c < f \ll (2\pi\tau)^{-1}$, since $\tau \sim 10^{-6}$–10^{-4} s). In addition, the Eq. 9 simplifies in such a way that the main electronic transport parameter is the carrier diffusion length.

The frequency range indicated above does not necessarily imply that the thermal response corresponds to the thermally thick regime, but can be close to it. Low

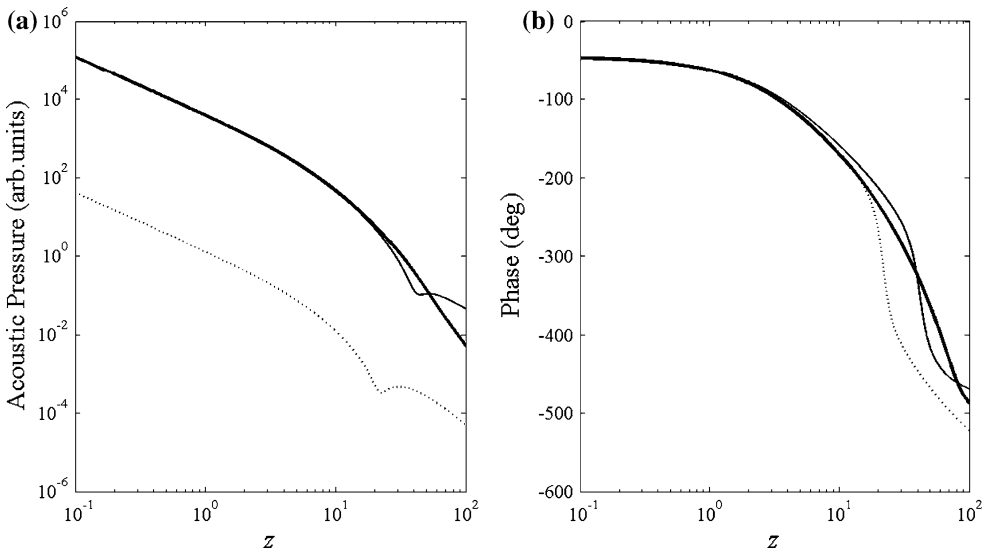

Fig. 2 Theoretical predictions for: **a** the amplitude and **b** phase difference of the acoustic pressure versus z for a-coefficient values of 1 (*dotted line*), 7 (*thin line*) and 10 (*thick line*)

Table 1 Group of studied samples and some of its physical characteristics

Sample	Bulk material	Type	Orientation	Thickness (μm)	Front surface	Rear surface
A1	Silicon	*n*	111	499	Etched	Polish
A2			100	482	Roughened	Roughened
A3				322	Etched	Polish
A4	Silicon	*p*	100	324	Etched	Polish
A5				372	Polish	Polish
A6				481	Roughened	Roughened

modulation frequencies values can make the sample thermally thin so that the thermal response do not depend on the thermal diffusivity, and performing PA measurements becomes difficult because the strong frequency dependence of the transduction system. On the other hand, for high modulation frequencies values, the signal to noise ratio is too small, diminishing the reliability of the measure.

Under the previous considerations, a much more simple expression for the acoustic pressure can be obtained:

$$\Delta P_{\mathrm{b}} \cong P_0 \frac{F}{z \sinh \sigma_{\mathrm{s}} l_{\mathrm{s}}} \tag{15}$$

where:

$$F = 1 + \frac{E_{\mathrm{g}}}{\Delta E}\left[1 - \left(\frac{\mu_\beta}{\mu_{\mathrm{D}}}\right)^2\right] \tag{16}$$

The Eq. 15 can be used as fitting function in a practical way. In this paper, this special case is named as the non-diffusive regime.

Experimental results

The studied samples are a group of six crystalline Si samples of different thicknesses, three of them are *n*-type, designated as A1, A2 and A3, and the rest are *p*-type, designated as A4, A5 and A6. Table 1 shows some physical characteristics of these samples.

Table 2 Set of electronic parameters of the samples

Sample	Bulk concentration (cm^{-3})	Mobility ($cm^2\ v^{-1}\ s^{-1}$)	Diffusion coefficient[a] ($cm^2\ s^{-1}$)
A1	-1.6×10^{15}	1.2×10^3	31.0
A2	-8.0×10^{16}	7.1×10^2	18.4
A3	-3.7×10^{13}	1.2×10^3	31.0
A4	8.9×10^{15}	2.6×10^2	6.7
A5	9.8×10^{15}	2.5×10^2	6.5
A6	5.2×10^{13}	1.2×10^3	31.0

[a] Calculated by means of Einstein's formula $D = \kappa_{\mathrm{B}} T \mu_c / e$

Table 2 shows the values of some of the electronic parameters for the six samples, measured by means of a Hall Effect measurement system (ECOPIA HMS-3000). The calculated minority carriers diffusion coefficient, *D*, is included as well.

Figure 3 shows the experimental set up used for the PA measurements. For the optical excitation a 120 mW Ar^+ laser (Omnichrome 543-200 MA) was used and its monochromatic beam intensity was modulated, at a frequency *f*, by a mechanical chopper SR-540 (Stanford Research Systems) before it normally impinges on the surface of the sample. The transducer consisted on a mono directional microphone, with wide 3 Hz–1.5 kHz flat frequency response. The PA signal was detected by a lock-in amplifier SR-850 (Stanford Research Systems), interfaced with a personal computer which allow recording the amplitude and phase of the PA signal as function of the modulation frequency.

Figures 4 and 5 show the experimental data of the PA signal versus modulation frequency for samples A2 and A6, respectively, obtained by means of the PA technique in a heat transmission configuration in the modulation frequency region 100 Hz $< f <$ 400 Hz. The PA measurements corresponding to the other four samples were performed too, but their graphs are not included here for better visualization.

The circles in Figs. 4 and 5 represent the experimental points and the solid lines are the best least squares fit of Eq. 15 to the experimental data, taking f_{c}, and μ_{D} as adjustable parameters.

Table 3 summarizes the fitted values of f_{c} and μ_{D}, as well as obtained values for τ. The non-linear fitting calculations were performed within a confidence band of 95%. In this form, the results obtained with Eq. 15 show a good agreement with those quoted in literature [12–14].

Conclusions

The fit of the model here described for the non-diffusive regime, Eq. 15, to the experimental data, provides values for the thermal diffusivity, the carrier's diffusion length

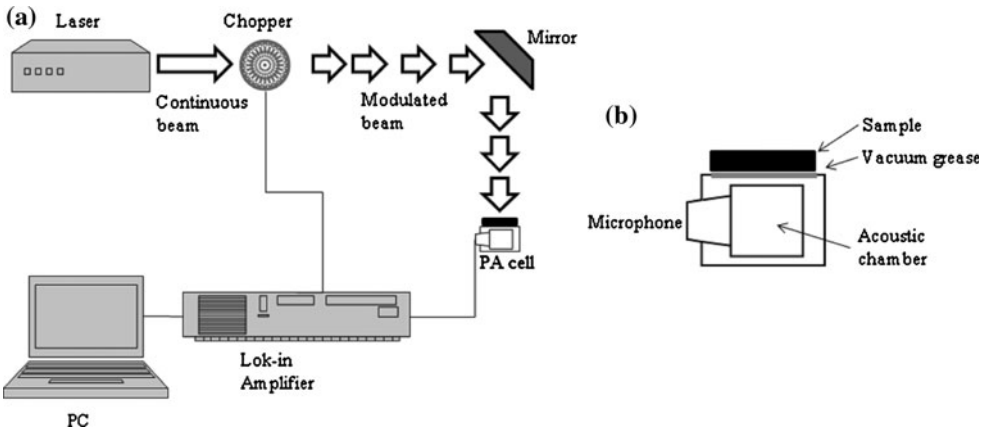

Fig. 3 Schema of the transmission configuration PA measurement system: **a** Experimental setup, **b** PA cell

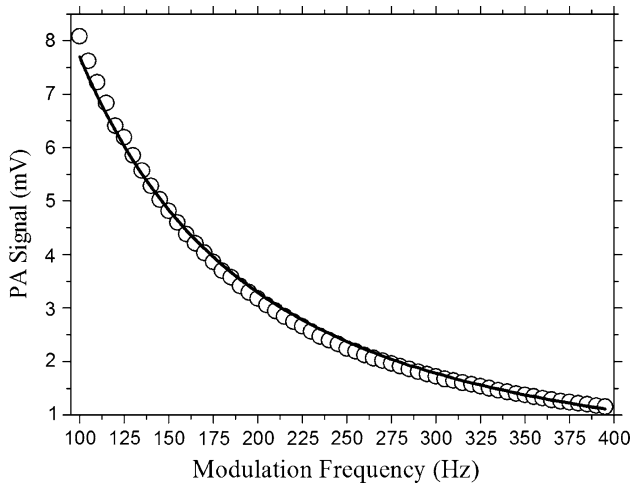

Fig. 4 Photoacoustic signal vs. modulation frequency of sample A2 (*n*-type). The *solid line* represents the best least squares fit of Eq. 15 to the experimental data

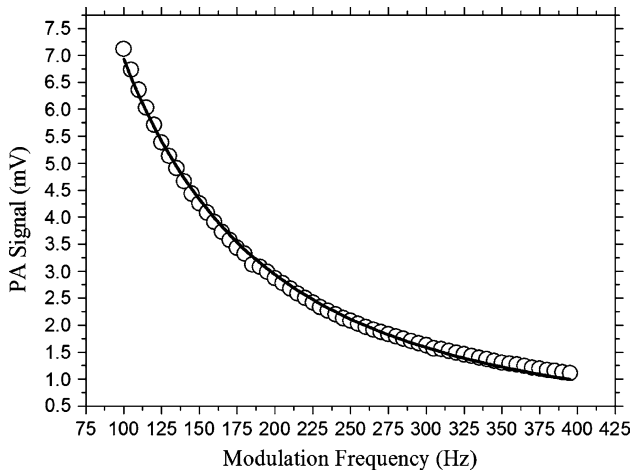

Fig. 5 Photoacoustic signal vs. modulation frequency of A6 sample (*p*-type). The *solid line* represents the best least squares fit of Eq. 15 to the experimental data

Table 3 Set of fitted values obtained by means of our model, in the non-diffusive regime approximation

Sample	Type	f_c (Hz)	μ_D (μm)	τ (μs)
A1	*n*	112.8	74.6	1.8
A2		120.8	43.5	1.0
A3		272.9	70.1	1.6
A4	*p*	269.5	82.7	10.2
A5		204.4	36.6	20.6
A6		122.7	37.9	0.4

and the total recombination lifetime that agree very well with those quoted in literature. One of the more remarkable properties of this model is its simplicity. Contrary to the commonly used models, were there are many adjustable parameters, the number of adjustable parameters in Eq. 15 is just two, which means a more fast and reliable calculation during the fitting procedure. The other major advantage that this equation brings is that it avoids the need of a special preparation of the sample (such as coating layers to eliminate the carrier transport processes and the corresponding extra photoacoustic measurements).

Acknowledgements This work was supported in part by Consejo Nacional de Ciencia y Tecnología (CONACYT), México, Secretaría de Investigación y Posgrado del Instituto Politécnico Nacional (SIP-IPN) and Comisión de Operación y Fomento de Actividades Académicas del Instituto Politécnico Nacional (COFAA-IPN), México.

References

1. Rosencwaig A, Gersho A (1976) J Appl Phys 47:64
2. Miranda LCM (1982) Appl Opt 21(16):2923
3. Fournier D, Boccara AC, Skumanich A, Amer NM (1986) J Appl Phys 59(3):787
4. Cheng JC, Zhang SY, Lu YS, Wang ZQ (1992) In: Bicanic D (ed) Photoacoustic and photothermal phenomena III, vol 69. Springer-Verlag, Berlin, Heidelberg, p 423
5. Pinto Neto A, Vargas H, Leite NL, Miranda LCM (1990) Phys Rev B 41(14):9971

6. Dramicanin MD, Ristovski ZD, Nicolic PM, Vasiljevic DG, Todorovic DM (1995) Phys Rev B 51(20):14226
7. González-T MA, Cruz-Orea A, Albor-A M de L, Castillo-A F de L (2005) Thin Solids Films 480–481:358
8. Todorovic DM, Nikolic PM (1997) Opt Eng 36(2):432
9. Marín E, Riech I, Díaz P, Alvarado-Gil JJ, Mendoza-Alvarez JG, Vargas H, Cruz-Orea A, Vargas M (1998) Phys Status Solidi a 169:275
10. Marín E, Calderón A, Riech I (2009) In: Marín Moares E (ed) Thermal wave physics and related photothermal techniques: basic principles and recent developments. Transworld Research Network, Kerala, India, p 159
11. Calderón A, Muñoz Hernández RA, Tomás SA, Cruz-Orea A, Sánchez Sinencio F (1998) J Appl Phys 84(11):6327
12. Touloukian YS, Powell RW, Ho CY, Nicolau MC (1973) Thermo-physical properties of matter, vol 10. IFI/Plenum, New York, p 160
13. Grove AS (1964) Physics and technology of semiconductor devices. Wiley, New York, p 102
14. Sze SM (1969) Physics and technology of semiconductor devices. Wiley, New York, p 57